JOURNAL OF COMPUTATIONAL PHYSICS **134,** 216–230 (1997)
ARTICLE NO. CP975686

Spectral Simulations of Electromagnetic Wave Scattering

B. Yang, D. Gottlieb, and J. S. Hesthaven[1]

Division of Applied Mathematics, Brown University, Box F, Providence, Rhode Island 02912
E-mail: baolin@cfm.brown.edu; dig@cfm.brown.edu; jansh@cfm.brown.edu

Received December 2, 1996; revised March 4, 1997

This paper present a multidomain pseudospectral method for accurately solving Maxwell's equations in the time domain. The scheme is developed for computing scattering by two-dimensional smooth perfectly conducting objects like circular or elliptic cylinders in free space and utilizes a Fourier collocation method in the azimuthal direction and a multidomain Chebyshev collocation method in the radial direction. Proper absorbing boundary conditions are discussed and a new perfectly matched layer (PML) method in polar coordinates is constructed and shown to be superior to other PML methods. For the elliptic cylinders we propose to use a matched layer in connection with the multidomain approach and a cubic grid mapping. Numerical results of monochromatic electromagnetic scattering by circular and elliptic perfectly electrically conducting cylinders are presented. Comparisons between results obtained using the multidomain pseudospectral method and the finite-difference time domain method clearly illustrate the superiority of spectral methods in obtaining accurate values for the scattered fields and the bistatic radar cross section.

1. INTRODUCTION

The finite-difference-time-domain (FD-TD) method, so extensively used for computing electromagnetic scattering by general objects, suffers from the requirement of having 10–20 grid points per wavelength to obtain sufficiently accurate solutions of the scattered fields. Indeed, in cases of transient excitation of the scatterer one must often use a significantly denser grid. Such requirements inhibit the use of FD-TD methods for accurately computing electromagnetic scattering by electrically large objects and transient phenomena.

On the other hand, it is well known [1] that the Fourier spectral method requires only two points per wavelength while the Chebyshev spectral method needs approximately π points per wavelength to accurately resolve a wave. Hence, using spectral methods for the solution of scattering problems promises a very significant decrease in the required number of grid points compared to FD-TD methods while maintaining the accuracy in time and space. This again suggests that spectral methods are very well suited for the simulation of electrically large or transient problems in electromagnetics [2–4].

Traditional spectral methods suffer from having a fixed distribution of grid points, thereby making it difficult to apply such methods for solving problems with strong internal layers or problems in complex geometries. Using a multidomain approach, i.e., splitting the computational domain into several geometrically simple body conforming domains, has proven to be a powerful way of overcoming these restrictions on the applicability of spectral methods (see, e.g., [5]). Moreover, such an approach allows for an efficient implementation on contemporary parallel computers [6] and relieves much of the computational burden of spectral methods even on serial computers, since one can increase the number of subdomains rather than the number of points in each subdomain resulting in a significant decrease in the total computational cost; see, e.g., [7].

In the present work we propose a multidomain pseudospectral method for accurately solving the time domain Maxwell's equations. The scheme is developed to demonstrate the accurate computation of scattering by smooth perfectly conducting two-dimensional objects in free space and utilizes a Fourier collocation method in the azimuthal direction and a multidomain Chebyshev collocation method in the radial direction. Besides demonstrating the efficacy of pseudospectral multidomain methods for addressing scattering problems we shall also show that such an approach has several additional advantages.

One of the most important, and as yet unsolved, problems in computational electromagnetics is the issue of obtaining solutions of infinite domain problems from finite domain numerical computations. Truncation of the computational domain introduces an artificial boundary and the crucial issue is how to design absorbing boundary conditions (ABC) such that outgoing waves are absorbed without reflections which may otherwise re-enter the domain and falsify the computational results.

A characteristic type ABC, requiring the incoming characteristic variable to vanish at the boundary, has often been used with high order methods. In [4], Kabakian proposed a single-domain spectral algorithm for electromagnetic wave

[1] Corresponding author.

0021-9991/97 $25.00

scattering, using a characteristic type boundary condition and satisfying results at early stages of the time integration (5–6 wave periods) were presented. However, we shall show that applying a characteristic type boundary condition causes significant reflections from the outer boundary, unless the outer boundary is put very far away from the scatter, i.e., at a distance of 12–20 wavelengths from the scatter.

As a very attractive alternative to the characteristic ABC, Berenger [8] proposed a perfectly matched layer (PML) method for reflectionless truncation of FD-TD wave simulations, with the property that the nonphysical absorbing layer is reflectionless, regardless of the angle of incidence and the frequency of the wave, although one should recall that the effectiveness of the layer in actual computations depends on the width of the absorbing layer utilized in the simulation. However, it was recently shown [9] that the split-field equations utilized in the PML are only weakly well-posed and may be explosively unstable under small perturbations, although this exponential growth has yet to be observed in most of the numerical experiments reported to date. We present a generalization of the PML method to polar coordinates which differs from those proposed in previous works [10–12]. This new polar PML is shown to admit plane wave solutions that match at a circular vacuum–layer interface, while decaying in any angle of propagation inside the layer.

For comparison, we give a direct implementation of the original rectangular PML method in the cylindrical computational domain and also consider an alternative way of applying the matched layer (ML) method, which involves a grid mapping and the use of high order filtering. The ML methods have the advantage that, unlike the PML methods, one only needs to solve Maxwell's equations with additional absorbing terms; i.e., it is applicable in any general curvilinear formulation of the Maxwell's equations, unlike the PML methods which require a rectangular interface.

The requirement for complex absorbing boundary conditions highlights yet another advantage of the multidomain approach as we may simply dedicate the outer subdomains to deal with such boundary conditions. Whether we need to solve equations different from Maxwell's equations, as in the PML methods, or we need to modify the equations with absorbing terms, as in the ML methods, everything is done locally in the domain being at the greatest distance from the scatter—we shall later refer to this domain as the absorbing layer subdomain. In the FD-TD implementation of the rectangular PML method [8], a small amount of numerical reflection at the vacuum–layer interface was observed. However, in a multidomain approach, derivatives are not computed across the vacuum–layer interface, thereby reducing the numerical reflections significantly.

In simulations of wave scattering by perfectly electrically conducting (PEC) circular cylinders, the new polar PML method is shown to yield the best results. Although the direct implementation of the rectangular PML method gives much better results than for the FD-TD methods, it is inferior to the new polar PML method by more than an order of magnitude. In simulations of wave scattering by PEC elliptic cylinders, we consider the use of the rectangular PML method and the ML method to find results of comparable accuracy for these particular cases.

The remaining part of the paper is organized as follows. In Section 2, we give the nondimensional Maxwell's equations and transformations. Section 3 discusses the basic properties of the proposed pseudospectral multidomain scheme, while Section 4 is devoted to a discussion of the absorbing boundary layer methods. In Section 5, numerical results validating the methods will be presented while concluding remarks are given in Section 6.

2. THE NONDIMENSIONAL MAXWELL'S EQUATIONS

We consider the two-dimensional transverse magnetic (TM) mode for which Maxwell's equations become

$$\frac{\partial \tilde{W}}{\partial \tilde{t}} = \tilde{A}\frac{\partial \tilde{W}}{\partial \tilde{x}} + \tilde{B}\frac{\partial \tilde{W}}{\partial \tilde{y}}, \tag{1}$$

where $\tilde{W} = (\tilde{H}_x, \tilde{H}_y, \tilde{E}_z)^{\mathrm{T}}$ with $\tilde{H}_x$, $\tilde{H}_y$, and $\tilde{E}_z$ being respectively the magnetic field components in the $\tilde{x}$ and $\tilde{y}$ directions and the electric field component normal to the domain of calculation and

$$\tilde{A} = \begin{pmatrix} 0 & 0 & 0 \\ 0 & 0 & \dfrac{1}{\mu_0} \\ 0 & \dfrac{1}{\varepsilon_0} & 0 \end{pmatrix}, \quad \tilde{B} = \begin{pmatrix} 0 & 0 & -\dfrac{1}{\mu_0} \\ 0 & 0 & 0 \\ -\dfrac{1}{\varepsilon_0} & 0 & 0 \end{pmatrix}. \tag{2}$$

Here ε_0 and μ_0 are the free space permittivity and permeability, with the speed of light in free space being $\tilde{c} = (\varepsilon_0\mu_0)^{-1/2}$.

The system can be nondimensionalized through the change of variables,

$$x = \tilde{x}/L, \quad y = \tilde{y}/L, \quad t = \tilde{c}\tilde{t}/L,$$

where L represents a length scale and the fields are normalized as

$$H_x = \tilde{H}_x, \quad H_y = \tilde{H}_y, \quad E_z = \sqrt{(\varepsilon_0/\mu_0)}\tilde{E}_z = Z_0^{-1}\tilde{E}_z,$$

where Z_0 represents the free-space impedance and we introduce the nondimensional vector, $W = (H_x, H_y, E_z)^{\mathrm{T}}$, to obtain the nondimensional and symmetric system,

$$\frac{\partial W}{\partial t} = A\frac{\partial W}{\partial x} + B\frac{\partial W}{\partial y}, \tag{3}$$

where

$$A = \begin{pmatrix} 0 & 0 & 0 \\ 0 & 0 & 1 \\ 0 & 1 & 0 \end{pmatrix}, \quad B = \begin{pmatrix} 0 & 0 & -1 \\ 0 & 0 & 0 \\ -1 & 0 & 0 \end{pmatrix}. \tag{4}$$

This form of the free-space Maxwell's equations is more convenient for analysis, as well as for computations, and is generally applicable when the material parameters are constant, it being the situation we have chosen to restrict our attention in the present work. One only needs to scale the physical fields initially and to transform them back after the final step of the time integration.

In general curvilinear coordinates the system (3) becomes

$$\frac{\partial \hat{W}}{\partial t} = \frac{\partial \hat{F}}{\partial \xi} + \frac{\partial \hat{G}}{\partial \eta} = \hat{A}\frac{\partial \hat{W}}{\partial \xi} + \hat{B}\frac{\partial \hat{W}}{\partial \eta}, \tag{5}$$

where $\hat{W} = JW$ with J being the transformation Jacobian,

$$J = x_\xi y_\eta - x_\eta y_\xi,$$

while

$$\hat{F} = J\begin{pmatrix} -\xi_y E_z \\ \xi_x E_z \\ \xi_x H_y - \xi_y H_x \end{pmatrix}, \quad \hat{G} = J\begin{pmatrix} -\eta_y E_z \\ \eta_x E_z \\ \eta_x H_y - \eta_y H_x \end{pmatrix}, \tag{6}$$

leading to

$$\begin{aligned} \hat{A} &= \frac{\partial \hat{F}}{\partial \hat{W}} = \begin{pmatrix} 0 & 0 & -\xi_y \\ 0 & 0 & \xi_x \\ -\xi_y & \xi_x & 0 \end{pmatrix}, \\ \hat{B} &= \frac{\partial \hat{G}}{\partial \hat{W}} = \begin{pmatrix} 0 & 0 & -\eta_y \\ 0 & 0 & \eta_x \\ -\eta_y & \eta_x & 0 \end{pmatrix}. \end{aligned} \tag{7}$$

We assume that $\xi_x^2 + \xi_y^2 = 1$ so that the eigenvalues of matrix $\hat{A}$ become

$$\lambda_1 = 0, \quad \lambda_2 = -1, \quad \lambda_3 = 1, \tag{8}$$

and we observe that $\hat{A}$ can be diagonalized by

$$S^{\mathrm{T}}\hat{A}S = \begin{pmatrix} 0 & 0 & 0 \\ 0 & -1 & 0 \\ 0 & 0 & 1 \end{pmatrix}, \quad S = \begin{pmatrix} \xi_x & \frac{\xi_y}{\sqrt{2}} & -\frac{\xi_y}{\sqrt{2}} \\ \xi_y & -\frac{\xi_x}{\sqrt{2}} & \frac{\xi_x}{\sqrt{2}} \\ 0 & \frac{1}{\sqrt{2}} & \frac{1}{\sqrt{2}} \end{pmatrix}.$$

The characteristic variables, $S^{\mathrm{T}}W$, are needed for applying characteristic boundary condition as we shall discuss shortly.

In polar coordinates we recover

$$\begin{aligned} \frac{\partial H_r}{\partial t} &= -\frac{1}{r}\frac{\partial E_z}{\partial \theta} \\ \frac{\partial H_\theta}{\partial t} &= \frac{\partial E_z}{\partial r} \\ \frac{\partial E_z}{\partial t} &= \frac{1}{r}\frac{\partial r H_\theta}{\partial r} - \frac{1}{r}\frac{\partial H_r}{\partial \theta}. \end{aligned} \tag{9}$$

3. THE COMPUTATIONAL SCHEME

The purpose of this paper is to demonstrate the efficacy of a pseudospectral multidomain approach for the simulation of electromagnetic wave scattering by smooth cylinders in free space. For this geometry it is natural to solve the problem in polar coordinates, Eq. (9). The solution is periodic in the azimuthal direction and the Fourier collocation method is suitable in this direction. The Chebyshev collocation method is used in the radial direction, and for the temporal discretization, a fourth-order Heun Runge–Kutta method [13] is used. High order filtering, a multidomain decomposition technique, and a cubic grid mapping technique are also employed, as we shall discuss shortly. A characteristic type boundary condition is applied at the scatter interface.

In the following, we describe the basic ingredients of the numerical scheme in polar coordinates.

• *The Fourier collocation method.* Given the values, $u(\theta_j)$, at the Fourier collocation points: $\theta_j = \pi j/N$, $j = 0, ..., 2N-1$, we seek an interpolating trigonometric polynomial of degree N,

$$I_N u(\theta) = \sum_{k=-N}^{N-1} \tilde{u}_k e^{ik\theta}, \tag{10}$$

where

$$\tilde{u}_k = \frac{1}{2N} \sum_{j=0}^{2N-1} u(\theta_j) e^{-ik\theta_j}, \tag{11}$$

and then we compute the derivative of the trigonometric polynomial,

$$(I_N u)'(\theta) = \sum_{k=-N}^{N-1} ik\tilde{u}_k e^{ik\theta}, \tag{12}$$

at the Fourier collocation points θ_j.

This procedure involves two FFT's, requiring $O(N \log_2 N)$ operations, one for the interpolation and one for the evaluation of the derivatives. We can also get the derivatives directly by a matrix–vector multiplication by noting that the interpolating Fourier series can be expressed in terms of a Lagrange interpolation polynomial.

• *The Chebyshev collocation method.* Given the values, $u(r_j)$, at the Chebyshev Gauss–Lobatto collocation points given as $r_j = \cos(\pi j/N), j = 0, ..., N$, we seek an interpolating polynomial of degree N,

$$I_N u(r) = \sum_{k=0}^{N} \tilde{u}_k T_k(r), \tag{13}$$

and compute the derivative of the polynomial,

$$(I_N u)'(r) = \sum_{k=0}^{N} \tilde{u}'_k T_k(r). \tag{14}$$

The coefficients, $\tilde{u}'_k$, are computed from the coefficients $\tilde{u}_k$ by using the backward recurrence relation

$$\begin{aligned} &\tilde{u}'_{N+1} = \tilde{u}'_N = 0, \\ &c_k \tilde{u}'_k = \tilde{u}'_{k+2} + 2(k+1)\tilde{u}_{k+1}, \quad k = 0, 1, ..., N-1, \end{aligned} \tag{15}$$

where

$$c_k = \begin{cases} 2, & \text{if } k = 0, \\ 1, & \text{otherwise.} \end{cases} \tag{16}$$

This procedure involves two CFTs, requiring $O(N \log_2 N)$ operations, one for the interpolation and one for the evaluation of the derivatives. We can also get the derivatives directly by a matrix–vector multiplication by noting that the interpolating polynomial can be expressed in terms of a Lagrange interpolation polynomial.

• *Filtering.* Given the Fourier series interpolation for $u(\theta)$,

$$I_N u(\theta) = \sum_{k=-N}^{N-1} \tilde{u}_k e^{ik\theta}, \tag{17}$$

we modify the original sum (17) as

$$u_N^{\sigma}(\theta) = \sum_{k=-N}^{N-1} \tilde{u}_k \sigma\left(\frac{k}{N}\right) e^{ik\theta}. \tag{18}$$

using the exponential filter,

$$\sigma\left(\frac{k}{N}\right) = e^{-\alpha(k/N)^m}, \tag{19}$$

where m is the order of the filter and $\alpha = -\log(\varepsilon)$ with ε being the machine zero. By choosing m to be proportional to N, we maintain the exponential accuracy of the spectral methods.

The filtering formula for the Chebyshev case is similar. The only difference is that the Fourier interpolation, Eq. (17), is replaced by the Chebyshev interpolation, Eq. (13).

• *Multidomain decomposition.* The multidomain decomposition method has been successfully used with spectral methods to deal with wave problems in complex geometries [5]. In the present application, the multidomain decomposition technique is used to allow for the implementation of various types of absorbing boundary conditions in the absorbing layer subdomain and to decrease the computational workload [7].

At the interface of any two subdomains, the characteristic relations are used to patch the field values. We enforce the characteristic variables along incoming characteristics in each subdomain to be the same as that along the outgoing characteristics in the neighboring subdomain. The zero speed characteristic variables are averaged across the interface and the outgoing characteristic variables are preserved. Denote by $C^+_{\xi,n}$, $C^-_{\xi,n}$, and $C^0_{\xi,n}$, $n = 1, 2$ (representing two neighboring subdomains), the characteristic variable values computed after any time step, corresponding to outgoing, incoming, and zero-speed characteristics, respectively, at the subdomains interface. Then we solve the following system to update the field values at the interface:

$$\begin{aligned} C^+_{\xi} &= C^+_{\xi,1}, \\ C^-_{\xi} &= C^-_{\xi,2}, \\ C^0_{\xi} &= \tfrac{1}{2}(C^0_{\xi,1} + C^0_{\xi,2}). \end{aligned} \tag{20}$$

Note that the unknowns are on the LHS and the RHS represent computed values. As we shall discuss in more detail in Section 4.2.3, the patching scheme is a little more complicated at the vacuum–layer interface when using

PML-type absorbing layers. However, the general idea of passing information along the characteristics remains the same also at such interfaces.

• *Cubic grid mapping.* For our implementations of the absorbing boundary conditions and the generation of an appropriate mesh outside an ellipse, a cubic grid mapping is adopted to map the Chebyshev Gauss–Lobatto collocation points r_j to points R_j, $j = 0, ..., N$, in an interval $[R_0, R_N]$ as desired, with the map being

$$R_j = C_1 \cdot (r_j + C_0)^3 + R_0 - C_1 \cdot (1 + C_0)^3, \qquad (21)$$

where

$$C_1 = \frac{R_N - R_0}{(C_0 - 1)^3 - (C_0 + 1)^3}, \quad j = 0, ..., N. \qquad (22)$$

The constant C_0 is free.

We shall find the cubic mapping useful in several aspects of the implementation of the absorbing layers as it allows for physically extending the absorbing layer subdomain in the radial direction while maintaining a high resolution at the vacuum–layer interface at no additional computational cost. The increased width of the absorbing layers yields an increased efficiency of the absorbing layers and results in the required additional accuracy commensurate with the use of pseudospectral methods as compared to more traditional FD-TD methods. We shall return to this topic in Section 4.1 and Section 4.2.3.

• *Boundary condition at the scatter.* Applying appropriate boundary conditions is crucial to the stability and accuracy of the collocation methods. As we are concerned with scattering by perfectly conducting bodies in free space, we shall find it useful to solve the problems in scattered field formulation [12] as described in more detail in Section 5. Hence, we shall only consider the case of Dirichlet boundary conditions by enforcing the physical boundary conditions of vanishing tangential electric field and normal magnetic field.

In the case of TM-scattering as considered here, we impose the exact boundary condition for E_z and apply the type of boundary treatments outlined for linear hyperbolic systems by Gottlieb *et al.* [14]; i.e., we use the characteristic relations to get the other field values. A similar treatment is applicable in the case of TE-scattering.

4. ABSORBING BOUNDARY CONDITIONS FOR MAXWELL'S EQUATIONS

A long-standing problem is computational electromagnetics has been the issue of finding infinite space solutions on a finite numerical domain. The issue is to prevent outgoing waves from being reflected from the artificial numerical boundaries.

In the following sections we shall discuss several schemes, among them some new methods, suitable for dealing with this problem in the context of electromagnetic scattering, and subsequently address the performance of the different methods through actual implementations of the various schemes.

4.1. The Characteristic and the ML Methods

The simplest type of absorbing boundary conditions, known as the characteristic boundary conditions, is enforced by imposing the incoming characteristic variable to be zero and has been used with spectral methods in previous applications [4]. This approach, however, is less well suited in connection with long time integration of Maxwell's equations using a spectral method as the following example shall illustrate.

Consider the plane wave solutions of the nondimensional Maxwell's equations, Eq. (3),

$$\begin{aligned} H_x &= \sin\phi e^{i\omega(t - x\cos\phi - y\sin\phi)} \\ H_y &= -\cos\phi e^{i\omega(t - x\cos\phi - y\sin\phi)} \\ E_z &= e^{i\omega(t - x\cos\phi - y\sin\phi)}, \end{aligned} \qquad (23)$$

with ϕ being the angle of propagation of the plane wave.

For a circular exterior boundary, one applies the characteristic boundary conditions by enforcing the incoming characteristic variable to be zero as

$$\sin\theta H_x - \cos\theta H_y + E_z = 0. \qquad (24)$$

For the plane wave solutions, Eq. (23), we have

$$\sin\theta H_x - \cos\theta H_y + E_z = (1 - \cos(\theta - \phi))e^{i\omega(t - x\cos\phi - y\sin\phi)}. \qquad (25)$$

Hence, this boundary condition is exact only if $\theta = \phi$, i.e., when the plane wave propagates perpendicular to the exterior boundary. The error in applying the characteristic type boundary condition is $O((\theta - \phi)^2)$.

One solution to this problem is to apply the multidomain approach and push the outer boundary of the absorbing layer subdomain sufficiently far away from the scatter. If r is large enough, the solution of electromagnetic wave scattering problems will be composed of plane waves with local direction $\phi \approx \theta$. In the multidomain formulation one may accomplish this by using a cubic grid mapping, Eq. (21), for the Chebyshev grid in the radial direction. This has the advantage of maintaining the computational workload while the grid in the radial direction transit gradually from

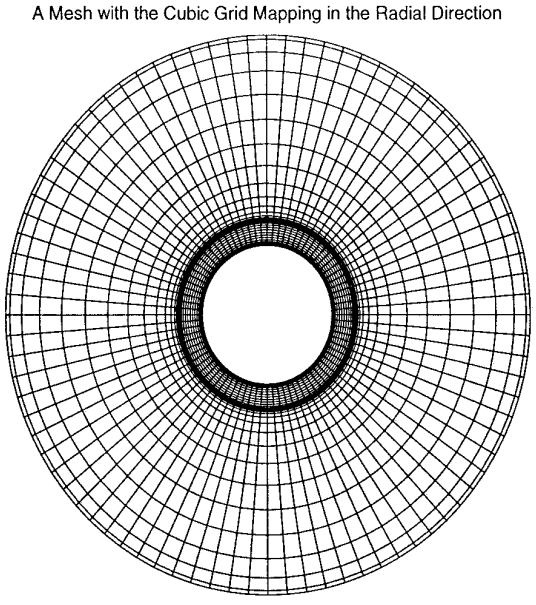

FIG. 1. A mesh utilizing a cubic grid mapping in the absorbing layer subdomain.

fine to coarse away from the scatter as illustrated in Fig. 1. The grid becomes so coarse near the outer boundary that the π points per wavelength rule [1] is violated. We find it to be necessary to apply a high order filter (Eq. (19), with the order of the filter m being close to N) following each time integration step to maintain stability of the scheme.

A better method is to combine the matched layer (ML) method with the grid mapping and the high order filtering technique. The ML method solves the nondimensional Maxwell's equations in the absorbing medium as

$$\frac{\partial W}{\partial t} = A\frac{\partial W}{\partial x} + B\frac{\partial W}{\partial y} - f(x,y)W, \tag{26}$$

where $f(x, y) \geq 0$ in the layer and $f(x, y) = 0$ at the vacuum–layer interface. The ML layer is put inside the absorbing layer subdomain at some distance from the subdomain interface and the cubic grid mapping is used to generate a mesh that is coarse in the part of the outer subdomain covered by the ML layer. Since a coarse mesh is used here, the number of grid points per wavelength decreases, and hence waves propagating into this area will appear as high frequency waves. With the help of a low pass filter, the reflections in the ML region, being of high frequency relative to the local grid, will be filtered out. Although the ML method certainly is simpler than the more elaborate PML methods which we introduce in the following section, they are found to perform well within the present context, i.e., considering monochromatic scattering by simple perfectly conducting objects. Moreover, there are no restrictions as to how exactly the ML is introduced into the computation; in particular the ML method is applicable in general curvilinear coordinates, although it is very important that the ML method be combined with the use of grid stretching and filtering. However, for more general polychromatic problems the performance of the ML methods remains unknown and we advocate that one uses the better understood PML methods for such problems.

The position of the ML layer, the conductivity profile of the layer (usually second to fourth order) and the cubic grid mapping can be tuned to reduce the reflections from the layer, much like tuning the PML layer as we shall see in the following.

4.2. The PML Methods

Ideally, an absorbing layer should be reflectionless with no dependence on the frequency and the direction of propagation of the waves. This is the purpose of the perfectly matched layer methods.

4.2.1. *The Rectangular PML Method*

In [8], Berenger proposed a PML method in rectangular coordinates. We present it here with some simple modifications. Consider the nondimensional PML type equations with spatially varying absorbing terms like

$$\begin{aligned}
\frac{\partial H_x}{\partial t} &= -\frac{\partial (E_{zx} + E_{zy})}{\partial y} - \mu_y H_x \\
\frac{\partial H_y}{\partial t} &= \frac{\partial (E_{zx} + E_{zy})}{\partial x} - \varepsilon_x H_y \\
\frac{\partial E_{zx}}{\partial t} &= \frac{\partial H_y}{\partial x} - \varepsilon_x E_{zx} \\
\frac{\partial E_{zy}}{\partial t} &= -\frac{\partial H_x}{\partial y} - \mu_y E_{zy},
\end{aligned} \tag{27}$$

where ε and μ are functions of x and y, respectively,

$$\varepsilon = \varepsilon(x), \quad \mu = \mu(y). \tag{28}$$

Formally, we have the following plane wave solutions to the above PML type equations:

$$\begin{aligned}
H_x &= \sin\phi e^{i\omega(t - x\cos\phi - y\sin\phi)} e^{-\varepsilon\cos\phi - \mu\sin\phi} \\
H_y &= -\cos\phi e^{i\omega(t - x\cos\phi - y\sin\phi)} e^{-\varepsilon\cos\phi - \mu\sin\phi} \\
E_{zx} &= \cos^2\phi e^{i\omega(t - x\cos\phi - y\sin\phi)} e^{-\varepsilon\cos\phi - \mu\sin\phi} \\
E_{zy} &= \sin^2\phi e^{i\omega(t - x\cos\phi - y\sin\phi)} e^{-\varepsilon\cos\phi - \mu\sin\phi}.
\end{aligned} \tag{29}$$

It is impotant that the solution is continuous across the

interface between the free space region and the PML region. This dictates that ε and μ must vanish on the interface boundary. If we also impose the condition that $\varepsilon_x(x)$ and $\mu_y(y)$ at the interface then the equations are well defined globally in free space, as well as inside the PML layer, and we have a set of plane wave solutions (29), decaying in the layer region for all frequencies, ω, and directions of propagation, ϕ, while remaining continuous across the vacuum–layer interface. Such solutions (29) will be referred to as matched plane wave solutions.

Let us assume that the PML region is outside a square bounded by $x = -a$, $x = a$, $y = -a$, and $y = a$. Then we can choose $\varepsilon(x)$ and $\mu(y)$ such that

$$\varepsilon(x) = C|x - a|^n, \quad n \geq 2, \tag{30}$$

outside the rectangular region and $\varepsilon(x) = 0$ inside the rectangular region. This choice ensures that $\varepsilon(x) = 0$, as well as $\varepsilon_x(x) = 0$, at the vacuum–layer interface. The choice for $\mu(y)$ is similar.

4.2.2. *The Polar PML Methods*

Recall the nondimensional Maxwell's equations in polar coordinates,

$$\begin{aligned}
\frac{\partial H_r}{\partial t} &= -\frac{1}{r}\frac{\partial E_z}{\partial \theta} \\
\frac{\partial H_\theta}{\partial t} &= \frac{\partial E_z}{\partial r} \\
\frac{\partial E_z}{\partial t} &= \frac{\partial H_\theta}{\partial r} + \frac{H_\theta}{r} - \frac{1}{r}\frac{\partial H_r}{\partial \theta},
\end{aligned} \tag{31}$$

with the plane wave solutions given as

$$\begin{aligned}
H_r &= H_x \cos\theta + H_y \sin\theta = -\sin(\theta - \phi) e^{i\omega(t - r\cos(\theta-\phi))} \\
H_\theta &= -H_x \sin\theta + H_y \cos\theta = -\cos(\theta - \phi) e^{i\omega(t - r\cos(\theta-\phi))} \\
E_z &= e^{i\omega(t - r\cos(\theta-\phi))}.
\end{aligned} \tag{32}$$

The extension of the PML method, proposed by Navarro *et al.* [11], results in the following split-field equations:

$$\begin{aligned}
\frac{\partial H_r}{\partial t} &= -\frac{1}{r}\frac{\partial (E_{zr} + E_{z\theta})}{\partial \theta} \\
\frac{\partial H_\theta}{\partial t} &= \frac{\partial (E_{zr} + E_{z\theta})}{\partial r} - g(r) H_\theta \\
\frac{\partial E_{zr}}{\partial t} &= -\frac{1}{r}\frac{\partial H_r}{\partial \theta} \\
\frac{\partial E_{z\theta}}{\partial t} &= \frac{\partial H_\theta}{\partial r} + \frac{H_\theta}{r} - g(r) E_{z\theta}.
\end{aligned} \tag{33}$$

We refer to this method as the Navarro polar PML method. This approach is also suggested by Rappaport in [10]. However, as we shall show through experiments, this method does not perform well in practice. We therefore suggest the split-field equations for the polar PML method,

$$\begin{aligned}
\frac{\partial H_r}{\partial t} &= -\frac{1}{r}\frac{\partial (E_{zr} + E_{z\theta})}{\partial \theta} - \frac{f(r)}{r} H_r \\
\frac{\partial H_\theta}{\partial t} &= \frac{\partial (E_{zr} + E_{z\theta})}{\partial r} - f'(r) H_\theta \\
\frac{\partial E_{zr}}{\partial t} &= \frac{H_\theta}{r} - \frac{1}{r}\frac{\partial H_r}{\partial \theta} - \frac{f(r)}{r} E_{zr} \\
\frac{\partial E_{z\theta}}{\partial t} &= \frac{\partial H_\theta}{\partial r} - f'(r) E_{z\theta},
\end{aligned} \tag{34}$$

where $f(r)$ is a function to be specified later.

It can be verified that these equations admit the following plane wave solutions:

$$\begin{aligned}
H_r &= -\sin(\theta - \phi) e^{i\omega(t - r\cos(\theta-\phi))} e^{-f(r)\cos(\theta-\phi)} \\
H_\theta &= -\cos(\theta - \phi) e^{i\omega(t - r\cos(\theta-\phi))} e^{-f(r)\cos(\theta-\phi)} \\
E_{zr} &= \sin^2(\theta - \phi) e^{i\omega(t - r\cos(\theta-\phi))} e^{-f(r)\cos(\theta-\phi)} \\
E_{z\theta} &= \cos^2(\theta - \phi) e^{i\omega(t - r\cos(\theta-\phi))} e^{-f(r)\cos(\theta-\phi)}.
\end{aligned} \tag{35}$$

Let the vacuum–layer interface be the circular boundary with $r = r_0$. Hence, we should have $f(r) = 0$ for $r < r_0$. Following the considerations of the absorbing and reflectionless properties of the polar PML method, $f(r)$ must satisfy the requirements

$$f(r_0) = 0 \tag{36}$$

and

$$f(r) > 0 \quad \text{for } r > r_0, \tag{37}$$

so that the plane wave solution decays for $r > r_0$. We also require that

$$f'(r) > 0 \quad \text{for } r > r_0. \tag{38}$$

An example of a valid choice of $f(r)$ is

$$f(r) = C(r - r_0)^n, \quad n = 1, 2, ..., r \geq r_0. \tag{39}$$

where C is a positive constant. This family of functions satisfies the requirements put forward in Eqs. (36)–(38).

One difference between the new polar PML method, Eq. (34), and the rectangular PML method, Eq. (27), is that the vacuum–layer interface of the former PML method is

a circle and can be represented by one grid line in polar coordinates, while the vacuum–layer interface of the rectangular PML method, Eq. (27), is a rectangle and is represented by four grid lines. The complexity of the interface of the rectangular PML method results in several regions of different properties inside the layer, which are not optimal for reflectionless wave absorption [8].

By looking at the decaying factor $e^{-f(r)\cos(\theta-\phi)}$ in Eq. (35), one observes that the plane wave solutions decay in the directions

$$|\phi - \theta| < \pi/2. \tag{40}$$

To get an idea of the rate of change of the magnitude of the wave, one may look at the directional derivative of the decaying factor.

LEMMA 4.1. *Let* $\mathbf{l} = (\cos\phi, \sin\phi)$ *be the normalized wave vector and assume that* $f(r)$ *satisfies the conditions* (37)–(38). *Then all plane waves decay in* every propagation direction *as*

$$\frac{\partial e^{-f(r)\cos(\theta-\phi)}}{\partial \mathbf{l}} < 0, \tag{41}$$

for any ϕ.

Proof.

$$\begin{aligned}
&\frac{\partial e^{-f(r)\cos(\theta-\phi)}}{\partial \mathbf{l}} \\
&= \cos\phi \frac{\partial e^{-f(r)\cos(\theta-\phi)}}{\partial x} + \sin\phi \frac{\partial e^{-f(r)\cos(\theta-\phi)}}{\partial y} \\
&= \cos\phi\cos\theta \frac{\partial e^{-f(r)\cos(\theta-\phi)}}{\partial r} - \cos\phi \frac{\sin\theta}{r} \frac{\partial e^{-f(r)\cos(\theta-\phi)}}{\partial \theta} \\
&\quad + \sin\phi\sin\theta \frac{\partial e^{-f(r)\cos(\theta-\phi)}}{\partial r} + \sin\phi \frac{\cos\theta}{r} \frac{\partial e^{-f(r)\cos(\theta-\phi)}}{\partial \theta} \\
&= \cos(\phi-\theta) \frac{\partial e^{-f(r)\cos(\theta-\phi)}}{\partial r} - \frac{\sin(\theta-\phi)}{r} \frac{\partial e^{-f(r)\cos(\theta-\phi)}}{\partial \theta} \\
&= -\left[\cos^2(\phi-\theta) f'(r) + \sin^2(\theta-\phi)\frac{f(r)}{r}\right] e^{-f(r)\cos(\theta-\phi)}.
\end{aligned} \tag{42}$$

Hence we have

$$\frac{\partial e^{-f(r)\cos(\theta-\phi)}}{\partial \mathbf{l}} < 0 \tag{43}$$

for any ϕ and any θ. ∎

The lemma emphasizes that all plane waves entering the PML layer decay exponentially along any direction of propagation inside the layer. The PML layer, however, does not extend to infinity and there will be reflections from the outer boundary of the truncated domain. In this case

$$|\phi - \theta| > \pi/2.$$

However, since r decreases now, these waves will also decay. Moreover, since

$$\cos^2(\phi-\theta) f'(r) + \sin^2(\theta-\phi)\frac{f(r)}{r} \geq \min\left(f'(r), \frac{f(r)}{r}\right) > 0, \tag{44}$$

for $r \geq r_0$, we have a lower bound for the rate of decay regardless of the direction of wave propagation ϕ, in the layer region away from the interface. We note that we cannot find such a lower bound for the rectangular PML, Eq. (27).

4.2.3. *PML Implementation Issues*

The calculations reported in this paper have been carried out using the multidomain approach, which is a very natural setting for the PML methods as the free space equations are solved in the inner subdomains while the PML equations are solved in the absorbing layer subdomain only. Note, however, that the free space domain has only three unknowns (H_x, H_y, and E_z in the rectangular case and H_r, H_θ, and E_z in the polar case), whereas the PML layer involves four unknowns (the electric field E_z is split into two; see Eqs. (27) and (34)), such that the patching conditions become less trivial. To overcome this difficulty we first observe that the PML system has the same number of positive and negative eigenvalues as the free space system, the extra eigenvalue being zero (this is exactly the reason why the PML system is only weakly well-posed [9]). We also observe that by adding and subtracting the third and fourth equations in Eq. (27) we recover Maxwell's equations for H_x, H_y, and $E_{zx} + E_{zy}$ and the unknown $E_{zx} - E_{zy}$ comes in the first three equations as a lower order term, thus not affecting the eigenvalues and the eigenvectors of the system. We therefore use the characteristic boundary treatment to patch H_x, H_y, and $E_{zx} + E_{zy}$ in the PML subdomain with H_x, H_y, and E_z in its neighboring subdomain, and we patch H_r, H_θ, and $E_{zr} + E_{z\theta}$ in the PML subdomain with H_r, H_θ, and E_z in its neighboring subdomain in the polar case.

The above discussion indicates the importance of imposing $\varepsilon_x(x) = \mu_y(y) = 0$ along the interface in the rectangular case and $f'(r)|_{r=r_0} = 0$ in the polar case. For the polar PML method, one can choose the functions in Eq. (39) with $n \geq 2$ and the constant C can be tuned for specific computations. Note that $f(r)/r$ and $f'(r)$ appear in the differential equations and need to be computed.

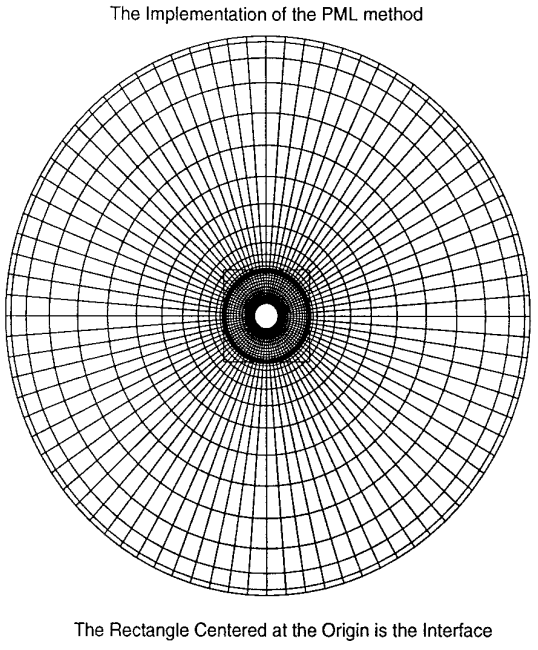

FIG. 2. An example of a mesh with an embedded rectangular interface suitable for the direct implementation of the rectangular PML method on the polar grid.

To apply the rectangular PML method in the polar coordinates considered in this work, a rectangular interface is fitted inside the absorbing layer subdomain of the multidomain mesh (see Fig. 2 for a typical 2-domain grid and the embedded rectangular interface). The accuracy and efficiency of the PML method depends critically on the size of the absorbing layer, i.e., the area outside the rectangular interface in Fig. 2. This is a particular concern in connection with high order methods as the efficiency of the absorbing layer has to match the accuracy of the overall scheme. To increase the total area of the absorbing layer we apply the cubic mapping, Eq. (21), as in the case of the ML method, to stretch the absorbing layer subdomain in the radial direction without sacrificing the accuracy of the overall scheme close to the vacuum–layer interface.

For the rectangular PML we choose

$$\varepsilon(x) = C|x - x_0|^n, \quad \mu(y) = C|y - y_0|^n. \tag{45}$$

The constant C can be tuned, $x = x_0, y = y_0$ is the interface, and n is an integer (usually 2–4), much as in the case of the ML scheme discussed in Section 4.1. These functions have gradual transition from 0 at the interface and we have found that, although by increasing n we can increase the order of smoothness at the interface, the overall absorption strength of the PML layer decreases, since it is proportional to the area between the profile and the x axis. Note that the maximum norm of $\varepsilon(x)$ and $\mu(y)$ should be bounded by some constant for stability consideration.

To test the reflecting and absorbing properties of the PML method, the layer is backed up by a perfect electric conductor by imposing $E_z = 0$ at the outer boundary. However, any ABC that is appropriate for the PML type equation can be applied at the outer boundary; e.g., characteristic type boundary conditions can be straightforwardly applied at the outer boundary.

5. NUMERICAL EXPERIMENTS

To show the efficacy of the multidomain pseudospectral methods for the simulation of electromagnetic wave scattering, as well as the efficacy of the proposed absorbing boundary conditions, we have implemented the methods discussed in the previous sections.

We shall consider simulation of two-dimensional TM wave scattering by perfectly conducting circular and elliptic cylinders. Due to the linearity of Maxwell's equation, we only compute the purely scattered field by using the boundary condition

$$E_{sc} = -E_{inc}, \tag{46}$$

at the cylinder surface.

Denote the radius of the circular cylinder by a and the wave number of the incident wave by k. The complexity of the problem increases with the frequency of the incident wave; e.g., the dynamic range for scattering by a circular PEC cylinder of electrical size $ka = 21\pi$ is about 30 dB, while the dynamic range for scattering by an elliptic PEC cylinder (major axis = 0.5 m, minor axis = 0.1225 m and $k = 42\pi$) is about 35 dB.

To assess the accuracy of the overall scheme in combination with one of the absorbing layer methods discussed in the previous sections, we shall also compute the scattering using a traditional rectangular FD-TD method (see, e.g., [12]), with the rectangular PML method, Eq. (27), as the absorbing boundary condition. However, to maintain a comparable accuracy in the rectangular FD-TD simulations we shall need meshes of substantially larger size. In the FD-TD method, the perfectly conducting cylinder is modeled as a cylinder with the permitivity being equal to that of free space but with a very high conductivity.

The radar cross section (RCS) is adopted as a main criterion for assessing the accuracy of the calculation of different schemes. A near-to-far-field transformation is used to get the far-field RCS from the near-field values [12]. The RCS is validated in two ways. The near-to-far-field transformation and the corresponding RCS computed along different closed contours should be the same up to numerical error. We also evaluate the RCS in the case of

scattering by a circular cylinder using the infinite series analytical solution [15] and refer to this RCS as "exact."

In our presentation of the RCS results, the bistatic RCSs are plotted in cylindrical form or angle-dB form, whichever yields more information. In order to see the difference in the backscatter region, being the most difficult to resolve, we cut the forward scatter region in many plots.

As convention for our pseudospectral multidomain mesh we use $l \times m \times n$, referring to l points in the azimuthal direction, m points in the radial direction and n subdomains of size $l \times m$ (1 for each subdomain).

5.1. Scattering by Circular Cylinders

The purpose of this section is to evaluate two issues raised in the previous discussion. The first of these involves the introduction and performance of the multidomain pseudospectral framework for the solution of two-dimensional TM scattering by perfectly conducting cylinders, as compared to the traditional FD-TD method.

The second issue concerns the relative merit of different absorbing layer techniques, among these the ML layer method, Eq. (26), the rectangular PML, Eq. (27), and a new polar PML method, Eq. (34). We shall attempt to arrive at an understanding of which of these methods is most useful in connection with the pseudospectral multidomain approach. This last issue is of significant importance to the accurate simulation of scattering. In previous work [4], however, the use of characteristic boundary conditions was advocated while in Section 4.1 we discussed the insufficiency of such an approach for long time integration. To illustrate this point, let us consider a simple example. To isolate the effects of the boundary condition we shall use a single domain Fourier–Chebyshev method with a characteristic boundary condition at the outer boundary. The electrical size of the cylinder is $ka = 7\pi$ (k: wave number and a: radius of the cylinder). The mesh we use is $84 \times 17 \times 1$ and the exterior boundary is placed three wavelengths away from the cylinder surface, a scenario similar to that used in [4]. To show the accuracy of this approach, the RCS results at different times are compared in Fig. 3. One clearly observes that the results are accurate before the reflections from the exterior boundary returns, after which the accuracy deteriorates in time, supporting the analysis of Section 4.1 and emphasizing the insufficiency of the characteristic type boundary condition for long time integration.

Let us now return to a comparison of the performance of the multidomain pseudospectral scheme and the rectangular FD-TD method with PML boundary conditions.

We shall present results obtained with a two-domain scheme only. However, several different computations with various numbers of subdomains have been completed, yielding results equivalent to the ones reported here for the two-domain case.

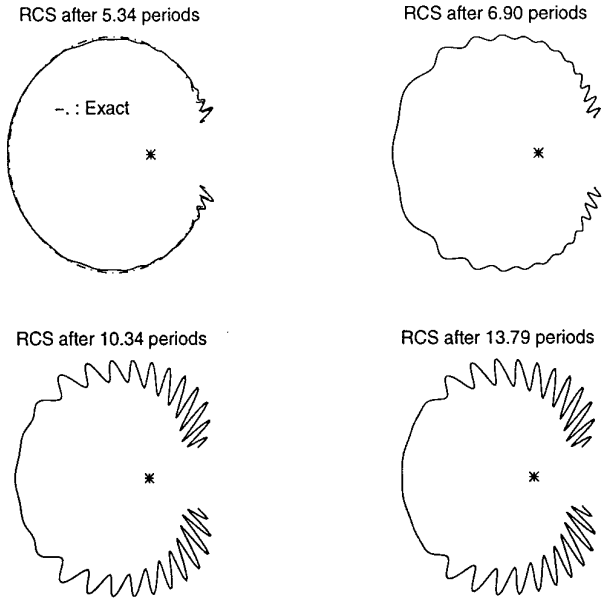

FIG. 3. Comparison of RCS's at different time for the one-domain Fourier–Chebyshev method with characteristic boundary condition. Electrical size of the cylinder is $ka = 7\pi$.

Consider first the problem of scattering by a circular cylinder with $ka = \pi$. In the multidomain simulations, the interface of the absorbing layers is $\frac{4}{3}$ of a wavelength away from the cylinder surface and we use a resolution of 18 Fourier modes and 17 Chebyshev modes in each subdomain. As the absorbing boundary condition we use either a direct implementation of the rectangular PML method, Eq. (27), the ML method, Eq. (26), or the new polar PML method, Eq. (34).

For the FD-TD solution, obtained using a rectangular FD-TD method with the rectangular PML method as an absorbing layer, we use a grid of the size 321×321, corresponding to 160 grid points per wave-length, with the vacuum–layer interface being about $\frac{4}{3}$ of a wavelength away from the scatter.

All the simulations are carried out over many wave periods to ensure that the RCS is stationary. In Table I, we compare the discrete L_2 error of the RCS and the computation time of the rectangular FD-TD method and the two-domain Fourier–Chebyshev methods. The computations are terminated after 30 wave periods for both the FD-TD method and the Fourier–Chebyshev methods.

Based on the results given in Table I, several conclusions may be made. Indeed, we find that comparing the accuracy as well as the computational efficiency supports the use of pseudospectral method for scattering problems. In particular, comparing the results obtained using the FD-TD method with PML boundary conditions (FD-TD-PML) with the results obtained using the multidomain scheme with the same boundary condition (FC-PML) we find that

TABLE I

Comparison of the Rectangular FD-TD Method with a 16-cell Rectangular PML Layer (FD-TD-PML) and the 2-Subdomain Fourier–Chebyshev Method with a Rectangular PML Layer (FC-PML), a ML Layer (FC-ML), or the New Polar PML Layer (FC-PPML)

Method	ka	Mesh	Discrete L_2 RCS error (dB)	CPU time (seconds)
FD-TD-PML	π	321×321	4.50E-2	1402
FC-PML	π	$18 \times 17 \times 2$	9.88E-3	37
FC-ML	π	$18 \times 17 \times 2$	6.26E-3	32
FC-PPML	π	$18 \times 17 \times 2$	6.40E-4	27

the latter is not only more accurate but also significantly faster. Moreover, the results in Table I also indicate that using the ML method in connection with the multidomain scheme (FC-ML) yields results comparable to those obtained with the rectangular PML method for this particular problem.

The best results are obtained by combining the new polar PML method, Eq. (34), with the multidomain scheme, being orders of magnitude better than those computed using the FD-TD method and obtained at a significantly lower computational cost.

In Fig. 4, we plot the RCS resulting from using the rectangular FD-TD method with the PML method and the Fourier–Chebyshev method with the rectangular PML for

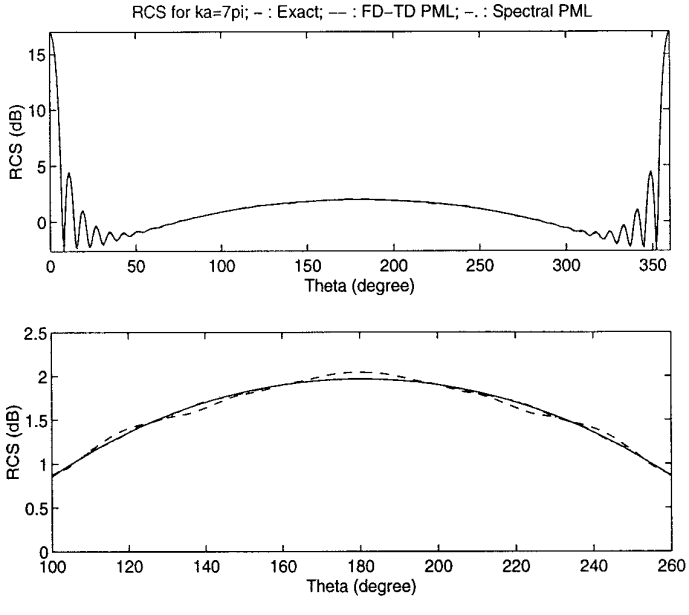

FIG. 4. RCS comparison for the FD-TD method and the pseudospectral multidomain method, both using the rectangular PML method. Electrical size of the cylinder is $ka = 7\pi$.

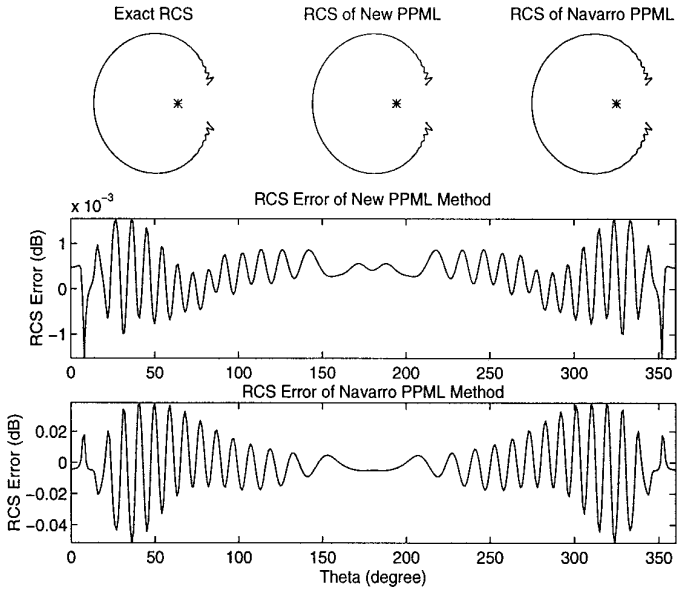

FIG. 5. RCS comparison for the new polar PML (PPML) method and the Navarro polar PML (PPML) method. Electrical size of the cylinder is $ka = 7\pi$.

simulating scattering from a cylinder of a larger electrical size as $ka = 7\pi$. For the pseudospectral multidomain time domain scheme using the rectangular PML method, we use an $84 \times 17 \times 2$ mesh. For the FD-TD method, we have to use a very fine grid, 1101×1101, to ensure a reasonable accuracy. The RCS resulting from the FD-TD method has obvious oscillation in the back scatter region while that of the spectral PML method agrees very well with the exact RCS. These results are consistent with those put forward in Table I illustrating the superiority of the pseudospectral multidomain scheme over the FD-TD method. It is therefore reasonable that using the polar PML method will produce even better results.

It seems clear that using a pseudospectral multidomain scheme for the solution of scattering problems results in an algorithm which is markedly more efficient as well as accurate as compared to the more traditional FD-TD scheme.

Next, we turn towards the performance of the new polar PML method, Eq. (34), and compare it to the PML method in polar coordinates suggested in [11], Eq. (33)], which we refer to as the Navarro polar PML method.

We consider again scattering by a circular cylinder of electrical size $ka = 7\pi$, and use a two-domain multidomain scheme with a standard Fourier–Chebyshev mesh of size $84 \times 17 \times 2$ for both cases.

In Fig. 5 we present the results of these two approaches. We find that the new polar PML method increases the accuracy substantially over the Navarro polar PML method. The discrete L_2 error of the RCS obtained using

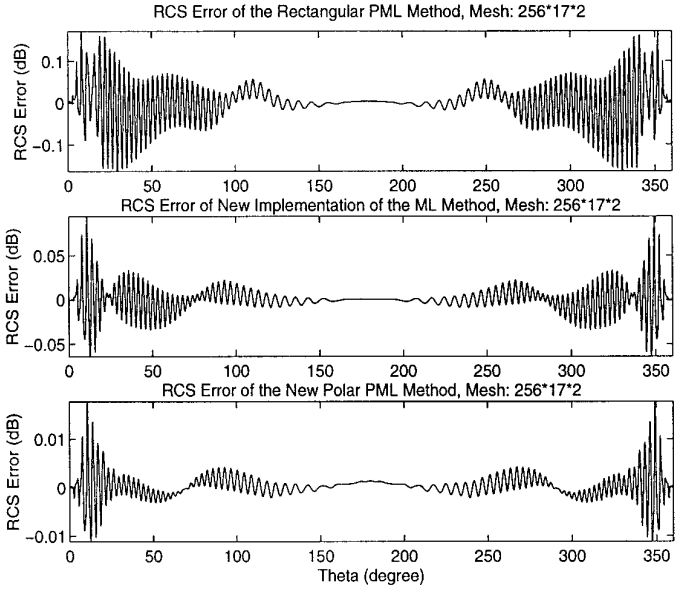

FIG. 6. RCS error plots of the rectangular PML method, the ML method, and the polar PML method. Electrical size of the cylinder is $ka = 21\pi$.

the new polar PML method is only 3.4% of that of the Navarro polar PML method. In our numerical experiments we also find that the best results with the Navarro polar PML method are obtained by using $g(r) = f_0'(r)$, with $f_0(r)$ being the best choice for the function $f(r)$ in the new polar PML method.

One of the prime arguments for considering the use of high-order methods, and in particular, spectral methods, is the ability to accurately obtain solutions to electrically large problems. Let us therefore consider the situation of high frequency scattering by a cylinder of size $ka = 21\pi$. This problem is out of the computational capacity of the FD-TD method on most computers, since a mesh larger than 2000×2000 should be used, this estimate being based on the accuracy obtained for the case of $ka = 7\pi$.

For the simulations of this electrically large-size scattering problem, we use the multidomain Fourier–Chebyshev method and one of several of the formerly introduced absorbing layer methods, i.e., the direct implementation of the rectangular PML, the new implementation of the ML method, or the new polar PML method. Irrespective of the choice of method, the computational domain is backed up by PEC ($E_z = 0$) at the outer domain boundary. The computational grid we use for all cases is $256 \times 17 \times 2$, i.e., just about two points per wavelength in the azimuthal direction.

In Fig. 6 we display a comparison of the RCS error for the three choices of absorbing boundary conditions considered here. We also solve the same problem using a very large mesh ($256 \times 17 \times 20$) and take this solution as the reference to obtain the normalized error of the scattered field, E_z. In Table II we compare the discrete L_2 error for both the RCS and the normalized error for the scattered field E_z as obtained using the three different types of absorbing boundary conditions.

From Fig. 6 as well as from Table II, it is clear that all three combinations of the scheme and the absorbing layer methods yield satisfying results for this problem, being nontrivial due to its large electrical size. However, it is also clear that the polar PML method, Eq. (34), outperforms the two alternatives, even though only the standard Fourier–Chebyshev mesh is used in its computation, i.e., we have not applied the mapping in this case to increase the total absorbing area, while this was found to be necessary for the ML method, as well as for the rectangular PML method, to arrive at results of accuracy comparable to that found with the polar PML method. We also note that the error of the ML method is only 20–30% of that of the direct implementation of the rectangular PML method.

Using the new polar PML method, an even more accurate result can be obtained by refining the mesh in the azimuthal direction. In this experiment, we use a $384 \times 17 \times 2$ mesh and get a better result for the RCS, as observed in Fig. 7. The highly oscillatory RCS is resolved to within 0.003 dB of the exact one.

It seems clear that the combination of the pseudospectral multidomain scheme and the new polar PML method yields an algorithm which is superior to the alternatives considered here in accuracy, as well as efficiency.

We should note that the introduction of several domains may seem as an unnecessary complication for the solution of the problems considered here. However, we remind the reader that the purpose here is to demonstrate the utility of the multidomain approach within computations of electromagnetic scattering. Having established that the multidomain approach suggested and studied here is stable and accurate supplies the foundation for the development of a more general pseudospectral multidomain scheme for the simulation of scattering by general two- and three-

TABLE II

Comparison of the Discrete L_2 Error Using a Pseudospectral Multidomain Scheme for the Computation of Scattering by a Cylinder of Size $ka = 21\pi$

Error	Method FC-PML	Method FC-ML	Method FC-PPML
Error for RCS (dB)	4.90E-2	1.54E-2	2.6E-3
Normalized error for E_z	3.50E-3	7.13E-4	1.41E-4

Note. We show the accuracy of the result obtained when using the rectangular PML method (FC-PML), the ML method (FC-ML) or the new polar PML method (FC-PPML), as the absorbing layer.

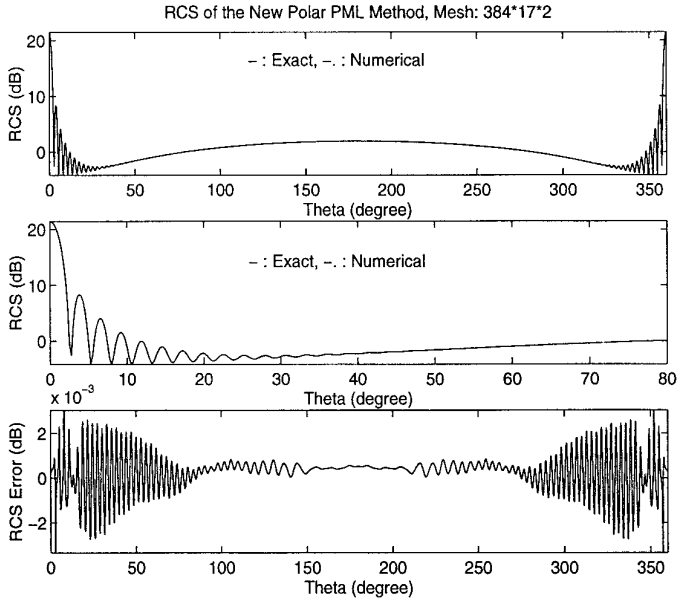

FIG. 7. RCS result of the polar PML method for a finer mesh. Electrical size of the cylinder is $ka = 21\pi$.

dimensional complex objects [16]. Moreover, within such a framework, provided the vacuum-layer is made circular, it is straightforward to apply the new polar PML method, Eq. (34).

5.2. Scattering by Elliptic Cylinders

To consider problems of a less trivial kind and of increased dynamics range, we present two simulations of electromagnetic wave scattering by elliptic cylinders. As boundary conditions we have used the direct implementation of the rectangular PML method or the ML method. By embedding a circular interface into the grid one could likewise use the new polar PML method as the absorbing boundary layer.

The elliptic cylindrical coordinates, (u, v), are related to the rectangular Cartesian coordinates, (x, y), by the transformation

$$\begin{aligned} x &= \tfrac{1}{2}d \cdot \cosh u \cdot \cos v, \\ y &= \tfrac{1}{2}d \cdot \sinh u \cdot \sin v, \end{aligned} \tag{47}$$

where $0 \le u < \infty$, $0 \le v < 2\pi$ and d is the interfocal distance. The scattering body is the elliptic cylinder with the surface $u = \text{const}$.

When the elliptic cylinder is fat, i.e., an aspect ratio about 1, one can use this transformation to generate the mesh outside the elliptic cylinder. However, when the elliptic cylinder is thin, the grid points generated by this transformation tend to cluster towards the cylinder surface, especially in the x direction. This induces an unwanted time step restriction in the computation, as well as loss of accuracy in regions where the mesh is coarse. The Chebyshev grid point distribution in the y direction tends to get too coarse away from the thin ellipse.

We consider, therefore, the following kind of modified transformation in our mesh generation,

$$\begin{aligned} x &= \frac{f(u)}{2} d \cdot \cosh u \cdot \cos v, \\ y &= \tfrac{1}{2}d \cdot \sinh u \cdot \sin v, \end{aligned} \tag{48}$$

where $f(u)$ is chosen to balance the grid-point distribution in the x direction and the y direction. We may also apply the cubic grid mapping in the inner domains to balance the grid distribution in the radial direction.

In the numerical experiments, waves of any angle of incidence and elliptic cylinders of different ratios between the major and minor axes are considered. Having made the validations for the circular cylinder case, we will use the result of a very large mesh ($l \times 17 \times 20$) as a reference, referred to as "exact." It is verified that the RCS obtained in different subdomains of the large mesh is almost invariant.

In the first simulation, the major axis of the ellipse is 0.5 m and the minor axis of the ellipse is 0.3808 m and we use only $l = 20$ Fourier modes in the azimuthal direction. The wave number of the incident wave is $k = 2\pi$. The angle of the incident wave is 45°. We use the multidomain Fourier–Chebyshev method with the direct implementation of the PML method as the absorbing boundary condition. See Fig. 8 for the mesh generated for this problem and note that we have used the cubic grid mapping in both subdomains. In Fig. 9, we give the RCS comparison. Note that the two-domain result is resolved to within 0.018 dB of the reference.

In the second simulation, the major axis of the ellipse is 0.5 m and the minor axis of the ellipse is 0.1225 m. The wave number of the incident wave is $k = 42\pi$ and we use $l = 256$ Fourier modes in the azimuthal direction. The angle of the incident wave is 45°. The dynamic range of this problem is about 35 dB, and the bistatic RCS is highly oscillatory. We use the ML method with the cubic grid mapping and solution filtering techniques for this simulation. The type of transformation given in Eq. (48) is also applied to generate the mesh for this problem; see Fig. 10. In Fig. 11 we show the RCS results. Note that the highly oscillatory RCS is resolved to within 0.2 dB of the reference.

6. CONCLUSIONS

The purpose of this paper has been twofold. The first objective was to introduce pseudospectral multidomain

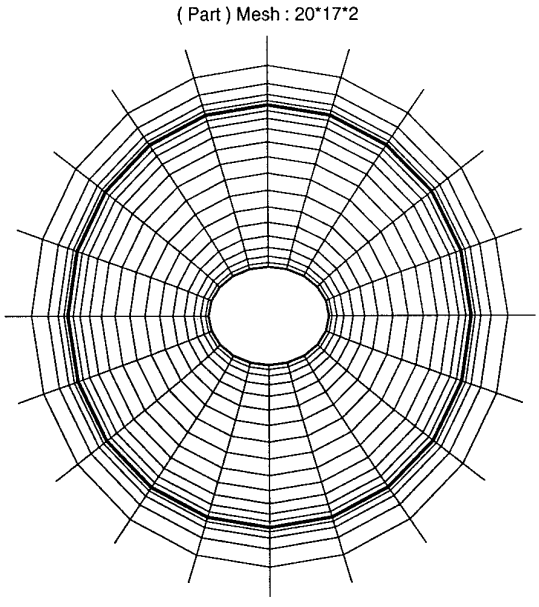

FIG. 8. The mesh used for simulating scattering from a mildly elliptic cylinder.

schemes for the accurate simulation of electromagnetic scattering by perfectly conducting objects. Indeed, it was shown that regarding accuracy as well as efficiency, such an approach has several things to offer over the more traditional FD-TD schemes. In the present work the main advantage of the multidomain framework remains the ease by which we may impose complicated absorbing boundary

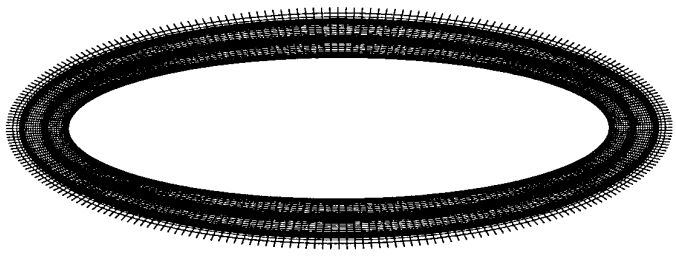

FIG. 10. The mesh part (256∗17∗3) used for simulating scattering from a strongly elliptic cylinder.

conditions in dedicated subdomains while at the same time resulting in a highly efficient algorithm in terms of required computational cost. However, more importantly, the demonstration and establishment of a stable and accurate pseudospectral multidomain framework opens up for the development of general purpose spectral algorithms for the solutions of scattering problems in arbitrary complex geometries. We are presently in the process of pursuing this issue further [16].

The second theme of this paper has been a detailed comparison of several schemes acting as absorbing boundary layers with the emphasis on identifying schemes that are sufficiently accurate to be applicable in a pseudospectral framework. It became clear, through analysis as well as computations, that the characteristic boundary condition yields only poor results, in particular for long time integration. Considering the rectangular PML method [8] as well as a new implementation of an ML method, we found that

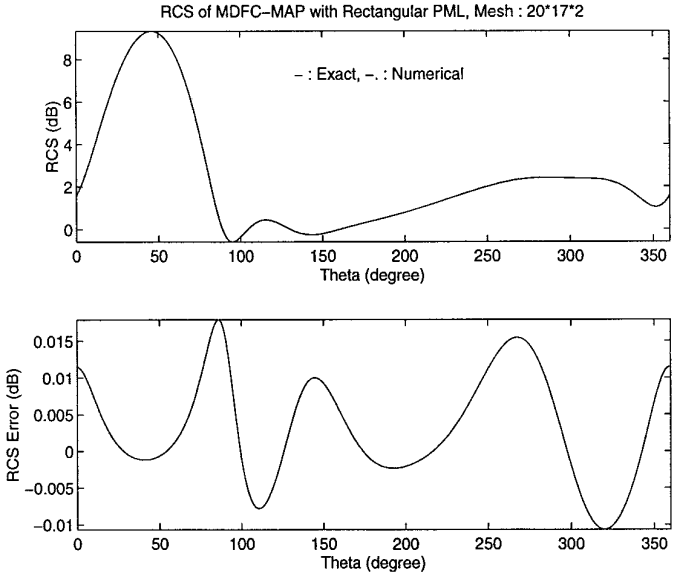

FIG. 9. RCS result from the multidomain pseudospectral method with the rectangular PML method for simulating scattering by a fat elliptic cylinder.

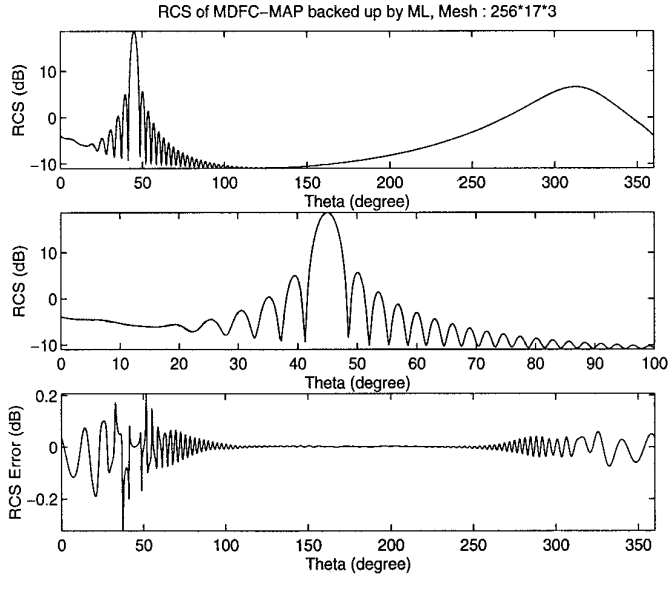

FIG. 11. RCS result from the multidomain pseudospectral method with the ML method for simulating scattering by a thin elliptic cylinder.

the results are generally of comparable accuracy, provided a cubic mapping is applied to increase the extension of the absorbing layer and, hence, increase the efficiency of the methods. Although the ML method has the advantage of being straightforward to impose in general coordinate systems, contrary to the rectangular PML scheme which requires a rectangular vacuum–layer interface, it remains unknown how the ML method will perform in a more general context, in particular, in a situation with polychromatic excitation.

We also introduced a new PML method in polar coordinates. Simulations indicate that the performance of this absorbing layer is superior to that of alternative PML methods, as well as the ML methods, when considering accuracy as well computational efficiency. Indeed, a circular vacuum–layer interface appears to be a very natural choice for two-dimensional scattering as does a sphere for the case of three-dimensional scattering. We are currently in the process of developing three-dimensional spherical PML methods and hope to report on this in the near future.

ACKNOWLEDGMENTS

The authors thank Peter G. Petropoulos for many helpful discussions and some useful codes. The first two authors were supported by DARPA/AFOSR Grant F49620-96-1-0426. The last author was also supported by DOE Grant DE-FG02-95ER25239 and NSF Grant ASC-9504002.

REFERENCES

1. D. Gottlieb and S. A. Orszag, Numerical Analysis of Spectral Methods: Theory and Applications, CBMS-NSF, Vol. 26 (Soc. Indus. Appl. Math., Philadelphia, 1977).
2. P. G. Petropoulos, Phase error control for FD-TD methods of second and fourth order accuracy, *IEEE Trans. Antennas Propag.* **42,** 859 (1994).
3. D. Gottlieb and B. Yang, Comparisons of staggered and non-staggered schemes for Maxwell's equations, in *Proc. of ACES 12th Annual Review of Progress in Applied Computational Electromagnetics, Monterey, 1996,* pp. 1122–1131.
4. A. V. Kabakian, A Spectral Algorithm for Electromagnetic Wave Scattering in the Time Domain Application to RCS Computation, in *Proc. of 27th AIAA Plasmadynamics and Lasers Conference, New Orleans, 1996.* [AIAA Paper 96-2334]
5. J. S. Hesthaven, A stable penalty method for the compressible Navier–Stokes equations. III. Multidimensional domain decomposition methods, *SIAM J. Sci. Comput.* [accepted]
6. P. Fischer and D. Gottlieb, On the Optimal Number of Subdomains for Hyperbolic Problems on Parallel Computers, *J. Supercomput. Appl.* [accepted]
7. J. S. Hesthaven, A Stable Penalty Method for the Compressible Navier-Stokes Equations. II. One Dimensional Domain Decomposition Method, *SIAM J. Sci. Comput.* **18,** 658 (1997).
8. J.-P. Berenger, A Perfectly Matched Layer for the Absorption of Electromagnetic Waves, *J. Comput. Phys.* **114,** 185 (1994).
9. S. Abarbanel and D. Gottlieb, A Mathematical Analysis of the PML Method, *J. Comput. Phys.* [accepted]
10. C. M. Rappaport, Perfectly Matched Absorbing Boundary Conditions Based on Anisotropic Lossy Mapping of Space, *IEEE Microwave Guided Wave Lett.* **5,** 94 (1995).
11. E. A. Navarro, C. Wu, P. Y. Chung, and J. Litva, Application of PML Superabsorbing Boundary Condition in the Non-orthogonal FD-TD Method, *IEE Electro. Lett.* **30,** 1654 (1994).
12. A. Taflove, Computational Electrodynamics—The Finite-Difference Time-Domain Method (Artech House, Boston, 1995).
13. C. Canuto, M. Y. Hussaini, A. Quarteroni, and T. A. Zang, Spectral Methods in Fluid Dynamics, Springer Series in Computational Physics (Springer-Verlag, New York, 1988).
14. D. Gottlieb, M. Gunzburger, and E. Turkel, On numerical boundary treatment for hyperbolic systems, *SIAM J. Numer. Anal.* **19,** 671 (1982).
15. J. J. Bowman, T. B. A. Senior, and P. L. E. Uslenghi, Electromagnetic and Acoustic Scattering by Simple Shapes (Hemisphere, New York, 1987).
16. B. Yang, D. Gottlieb, and J. S. Hesthaven, On the use of PML ABC's in spectral time-domain simulations of electromagnetic scattering, in *Proc. of ACES 13'th Annual Review of Progress in Applied Computational Electromagnetics, Monterey, 1997,* pp. 926–933.